

**Barlowite as a canted antiferromagnet: Theory and experiment**Harald O. Jeschke,<sup>1</sup> Francesc Salvat-Pujol,<sup>1</sup> Elena Gati,<sup>2</sup> Nguyen Hieu Hoang,<sup>2</sup> Bernd Wolf,<sup>2</sup> Michael Lang,<sup>2</sup> John A. Schlueter,<sup>3</sup> and Roser Valenti<sup>1</sup><sup>1</sup>*Institut für Theoretische Physik, Goethe-Universität Frankfurt, Max-von-Laue-Straße 1, 60438 Frankfurt am Main, Germany*<sup>2</sup>*Physikalisches Institut, Goethe-Universität Frankfurt, Max-von-Laue-Straße 1, 60438 Frankfurt am Main, Germany*<sup>3</sup>*Division of Materials Research, National Science Foundation, Arlington, Virginia 22230, USA*

(Received 19 December 2014; revised manuscript received 24 August 2015; published 10 September 2015)

We investigate the structural, electronic, and magnetic properties of the newly synthesized mineral barlowite  $\text{Cu}_4(\text{OH})_6\text{FBr}$  which contains  $\text{Cu}^{2+}$  ions in a perfect kagome arrangement. In contrast to the spin-liquid candidate herbertsmithite  $\text{ZnCu}_3(\text{OH})_6\text{Cl}_2$ , kagome layers in barlowite are perfectly aligned due to the different bonding environments adopted by  $\text{F}^-$  and  $\text{Br}^-$  compared to  $\text{Cl}^-$ . With the synthesis of this material we unveil a design strategy for layered kagome systems with possible exotic magnetic states. Density functional theory calculations and effective model considerations for  $\text{Cu}_4(\text{OH})_6\text{FBr}$ , which has a  $\text{Cu}^{2+}$  site coupling the kagome layers, predict a three-dimensional network of exchange couplings, which together with a substantial Dzyaloshinskii-Moriya coupling lead to canted antiferromagnetic ordering of this compound in excellent agreement with magnetic susceptibility measurements on single crystals yielding  $T_N = 15$  K.

DOI: [10.1103/PhysRevB.92.094417](https://doi.org/10.1103/PhysRevB.92.094417)

PACS number(s): 75.10.Jm, 71.15.Mb, 75.30.Cr, 75.30.Et

Since the successful synthesis of herbertsmithite [ $\text{ZnCu}_3(\text{OH})_6\text{Cl}_2$ ] [1], spin-liquid candidates based on spin-1/2 kagome lattices have been intensively investigated in recent years [2,3]. The paratacamite family of compounds has proven to be a fertile ground for kagome materials with different properties. The  $\text{Zn}_x\text{Cu}_{4-x}(\text{OD})_6\text{Cl}_2$  series of materials has been found to form valence-bond solids due to distortions of the kagome layer in monoclinic space groups [4]. The replacement of  $\text{Zn}^{2+}$  in  $\text{ZnCu}_3(\text{OH})_6\text{Cl}_2$  by a nonmagnetic ion, such as  $\text{Mg}^{2+}$ , possibly leads to another spin-liquid candidate [5] as does the replacement of  $2\text{Cl}^-$  by  $\text{SO}_4^{2-}$  [6]. On the other hand, magnetic ions between the kagome layers lead to compounds that order magnetically [7]. Although realizations of quantum spin liquids have been desperately searched for [8], so far, together with the triangular-lattice molecule-based organic materials [9,10], herbertsmithite has been considered one of the best candidates [11]. However,  $\text{ZnCu}_3(\text{OH})_6\text{Cl}_2$  has not been free from controversy as  $\text{Zn}^{2+}$  and  $\text{Cu}^{2+}$  are similar in size, and both kagome layers diluted with nonmagnetic  $\text{Zn}^{2+}$  [3] as well as magnetic  $\text{Cu}^{2+}$  ions replacing  $\text{Zn}^{2+}$  between the kagome layers [12] are possible. Therefore, it would be desirable to devise a crystal modification of herbertsmithite that would make the  $\text{Cu}^{2+}$  and  $\text{Zn}^{2+}$  sites less similar in order to increase the tendency of  $\text{Cu}^{2+}$  ions to form the kagome layer as well as the tendency of the nonmagnetic transition-metal ion to stay away from the kagome plane. Recently [13] one of the authors introduced the mineral barlowite  $\text{Cu}_4(\text{OH})_6\text{FBr}$  as a layered structure of two-dimensional (2D) Cu-based perfect kagome planes and reported the observation of antiferromagnetic order at low temperatures based on thermodynamic measurements on polycrystalline samples. In the present paper we go beyond previous studies and suggest a synthetic route to successfully obtain perfect kagome structures, exemplarily realized in the mineral barlowite. Such structures offer an important alternative to herbertsmithite. They are chemically and physically flexible enough so that via doping or application of pressure one can explore not only potential quantum spin-liquid behavior at half-filling, but also other exotic states, such as flat bands at certain fillings inducing

Nagaoka ferromagnetism [14] or the presence of Dirac points at 4/3 filling that could lead to unusual symmetry-protected metals or superconductors [15].

Furthermore, we resolve the microscopic origin of the electronic and magnetic behaviors of barlowite, which has a  $\text{Cu}^{2+}$  site coupling the kagome layers. Via a combination of density functional theory (DFT) calculations and magnetic susceptibility measurements we find this material to be a canted antiferromagnet below  $T < T_N$  with a canting angle away from the kagome plane of  $4.5^\circ$ .

In herbertsmithite, the  $\text{Cl}^-$  binding environment is partially covalent, partially hydrogen bonded, as shown in Fig. 1(a). This leads to a horizontal staggering of kagome layers [Fig. 1(b)] as  $\text{Cu}^{2+}$  triangles can be placed either above or below a  $\text{Cl}^-$  ion but not both above and below. We suggest using a mixed halide system where the strong hydrogen bond acceptance of the  $\text{F}^-$  ion is used to create a hydrogen-rich pocket with six hydroxyl ions; on the other hand,  $\text{Br}^-$  can form six covalent bonds to three  $\text{Cu}^{2+}$  ions above and three below [Fig. 1(c)]. Following this recipe via the chemical synthesis of  $\text{Cu}_4(\text{OH})_6\text{FBr}$ , we arrive at perfectly aligned kagome planes as shown in Fig. 1(d). This compound is known as the mineral barlowite [16].

Single crystals of barlowite  $\text{Cu}_4(\text{OH})_6\text{FBr}$  were grown synthetically through the hydrothermal reaction of copper carbonate basic (malachite), with perbromic acid in the presence of ammonium fluoride. The crystal structure of  $\text{Cu}_4(\text{OH})_6\text{FBr}$  was determined by single-crystal x-ray diffraction measurements [17] at ambient temperature and is shown in Fig. 2. Barlowite crystallizes in  $P6_3/mmc$  symmetry with each intralayer  $\text{Cu}^{2+}$  [Cu(1)] ion lying on a site of  $2/m$  symmetry (see Table I). This intralayer  $\text{Cu}^{2+}$  exhibits a strongly tetragonally distorted octahedral coordination with four equatorial Cu-O bonds of  $1.954(1)$  Å and two axial Cu-Br bonds of  $3.022$  Å. Interlayer  $\text{Cu}^{2+}$  [Cu(2)] sites lie on a general position and are thus 1/3 occupied and disordered over three equivalent positions.

In order to characterize barlowite electronically and magnetically, we combined first-principles DFT calculations with

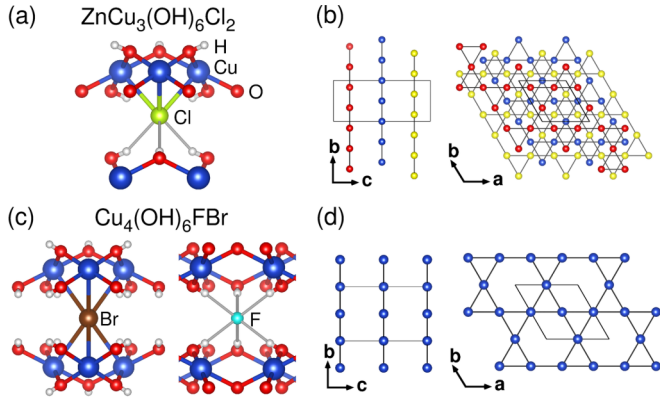


FIG. 1. (Color online) Chloride environment of (a) herbertsmithite compared to bromide and fluoride environments of (c) barlowite. (b) A mix of covalent and hydrogen bonding in  $\text{ZnCu}_3(\text{OH})_6\text{Cl}_2$  leads to three kagome layers shifted with respect to each other as shown by differently colored  $\text{Cu}^{2+}$  sites. (d) Preference of  $\text{Br}^-$  for covalent bonding and of  $\text{F}^-$  for hydrogen bonding leads to perfect alignment of kagome layers in  $\text{Cu}_4(\text{OH})_6\text{FBr}$  [only Cu(1) sites are shown here].

susceptibility measurements. Our DFT calculations were performed on the basis of the full-potential nonorthogonal local-orbital basis [18], employing the generalized gradient approximation (GGA) [19] as well as GGA +  $U$  [20] functionals. The Hubbard parameter  $U$  was set to 6 eV, and the Hund's rule coupling  $J_H$  was set to 1 eV. Note that for reasons of comparability with the closely related material herbertsmithite, we have here chosen the same values of  $U$  and  $J_H$  as in our previous study Ref. [21]. The exchange-coupling constants between spin-1/2  $\text{Cu}^{2+}$  ions were obtained by mapping GGA +  $U$  total energy differences of several  $\text{Cu}^{2+}$  spin configurations onto a spin-1/2 Heisenberg model [21,22]. In order to make a sufficient number of  $\text{Cu}^{2+}$  sites inequivalent to allow for various spin configurations, the symmetry was lowered from the  $Cmcm$  to the  $Cm$  space group (No. 8) containing six inequivalent  $\text{Cu}^{2+}$  positions.

In Figs. 3(a) and 3(b) we show first the GGA band structure and density of states of barlowite. The main contribution

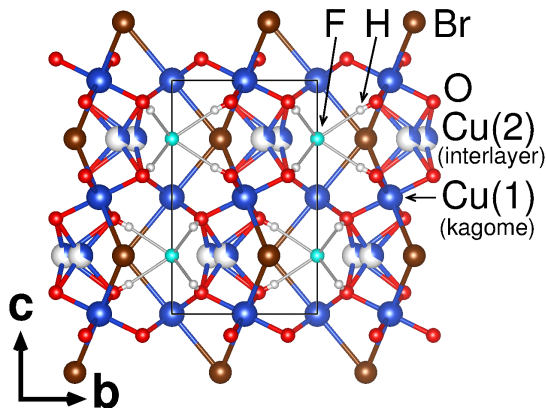


FIG. 2. (Color online) Crystal structure of  $\text{Cu}_4(\text{OH})_6\text{FBr}$  ( $P6_3/mmc$  space group, No. 194). Note that the Cu(2) site with Wyckoff position  $12j$  is  $\frac{1}{3}$  filled.

TABLE I. Structural parameters for  $\text{Cu}_4(\text{OH})_6\text{FBr}$  at  $T = 298(2)$  K [ $P6_3/mmc$  space group,  $a = 6.799(4)$ ,  $c = 9.3063(13)$  Å, and  $Z = 2$ ]. In this table,  $U$  is the anisotropic displacement parameter (isotropic for H).

| Atom  | Site | $x$           | $y$           | $z$           | $U$ (Å <sup>2</sup> ) | Occ.          |
|-------|------|---------------|---------------|---------------|-----------------------|---------------|
| Cu(1) | 6g   | $\frac{1}{2}$ | 0             | 0             | 0.01540(17)           | 1             |
| Cu(2) | 12j  | 0.62884(12)   | 0.2577(2)     | $\frac{1}{4}$ | 0.0133(4)             | $\frac{1}{3}$ |
| O     | 12k  | 0.79768(18)   | 0.20232(18)   | 0.0916(2)     | 0.0137(4)             | 1             |
| H     | 12k  | 0.852(3)      | 0.148(3)      | 0.127(4)      | 0.021                 | 1             |
| Br    | 2c   | $\frac{1}{3}$ | $\frac{2}{3}$ | $\frac{1}{4}$ | 0.0184(2)             | 1             |
| F     | 2b   | 0             | 0             | $\frac{1}{4}$ | 0.0238(10)            | 1             |

near the Fermi level is of Cu  $3d$  orbitals hybridized with O  $2p$  orbitals. The band structure along the high-symmetry path  $\Gamma$ - $M$ - $K$ - $\Gamma$  reflects the dispersion of the kagome layers [dominated by Cu(1)  $d$  states] whereas the band structure along the high-symmetry path  $A$ - $L$ - $H$ - $A$  at  $k_z = 0.5$  arises from the 2D lattice formed by the interkagome Cu(2) atoms. The electronic structure of the kagome layer resembles that of the spin-liquid compound herbertsmithite very well [21]. However, both herbertsmithite and barlowite are Mott insulators. In order to reflect this behavior in the band-structure calculations we show in Fig. 3(c) the density of states calculated with the GGA +  $U$  functional with  $U = 6$  eV.

The exchange couplings we obtain from total energy calculations are listed in Table II. The nearest-neighbor coupling

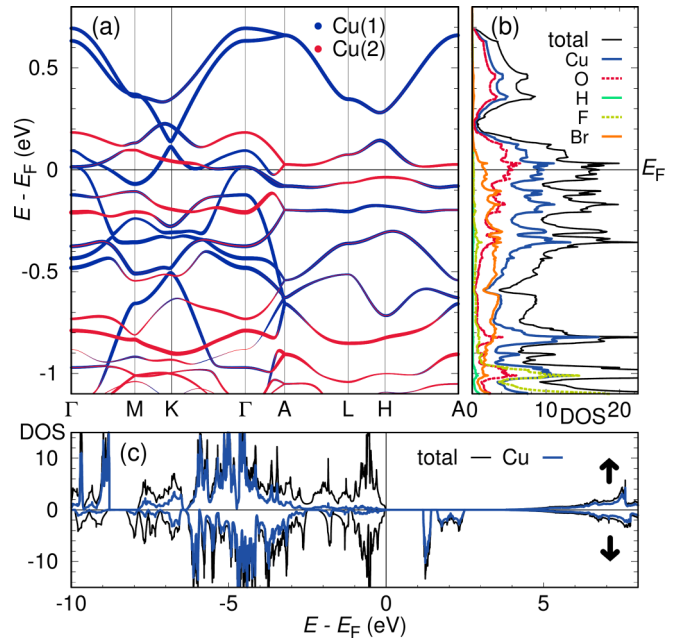


FIG. 3. (Color online) (a) GGA band structure and (b) GGA density of states (DOS) of  $\text{Cu}_4(\text{OH})_6\text{FBr}$ . DOS is given in states per eV and formula unit. High-symmetry points  $M = (\frac{1}{2}, 0, 0)$ ,  $K = (\frac{1}{3}, \frac{1}{3}, 0)$ ,  $A = (0, 0, \frac{1}{2})$ ,  $L = (\frac{1}{2}, 0, \frac{1}{2})$ , and  $H = (\frac{1}{3}, \frac{1}{3}, \frac{1}{2})$  were chosen to reflect the  $P6_3/mmc$  symmetry of the real material rather than the  $Cmcm$  symmetry used for computational purposes. (c) GGA +  $U$  density of states for  $U = 6$ ,  $J_H = 1$  eV and ferromagnetic order. Note that the size of the gap is related to the value of  $U$  considered.

TABLE II. Exchange-coupling constants for  $\text{Cu}_4(\text{OH})_6\text{FBr}$ , calculated with GGA +  $U$  at  $U = 6$  eV,  $J_H = 1$  eV and with atomic-limit double-counting correction. Positive (negative)  $J$  values denote antiferromagnetic (ferromagnetic) couplings.

| Name                  | $d_{\text{Cu-Cu}}$ (Å) | Type        | $J_i$ (K) |
|-----------------------|------------------------|-------------|-----------|
| Kagome layer coupling |                        |             |           |
| $J_3$                 | 3.3399                 | Cu(1)-Cu(1) | 177       |
| Interlayer couplings  |                        |             |           |
| $J_1$                 | 2.7632                 | Cu(1)-Cu(2) | -205      |
| $J_2$                 | 3.1885                 | Cu(1)-Cu(2) | -32       |
| $J_4$                 | 4.6532                 | Cu(1)-Cu(1) | 5         |
| $J_6$                 | 5.5264                 | Cu(2)-Cu(2) | 16        |

in the kagome plane is  $J_3 = 177$  K for barlowite. This is very similar to the value  $J = 182$  K obtained for herbertsmithite, reflecting the fact that Cu-O-Cu angles are very similar in both compounds ( $117^\circ$  in barlowite and  $119^\circ$  in herbertsmithite). The fact that barlowite has  $\text{Cu}^{2+}$  ions at interlayer positions [Cu(2)] determines the magnetic behavior of this system at low temperatures. Specifically, we find that ferromagnetic interlayer couplings ( $J_1 = -205$  and  $J_2 = -32$  K) exist between Cu(1) (in the kagome layer) and Cu(2) (interlayer). Further exchange paths become increasingly and significantly weaker—comparable or smaller than  $0.1J$ . Within the  $Cm$  unit cell chosen here, it was not possible to separate the coupling  $J_5$  corresponding to a Cu(1)-Cu(2) distance of  $5.2359$  Å from the small ferromagnetic  $J_2$ . The vertical coupling  $J_4$  between the kagome planes is negligibly small. The resulting Heisenberg Hamiltonian parameters are illustrated in Fig. 4. Note that due to the lowering of the symmetry from  $P6_3/mmc$  to  $Cmcm$  for the calculations, the path of the ferromagnetic one-dimensional Cu(2) chains has become uniquely defined. In reality, these chains wiggle through the crystal according to the actual positions of Cu(2), which is randomly chosen from the three possible sites. We estimate an error bar on the Heisenberg Hamiltonian parameters on the order of 20% and possibly larger for the smaller couplings because the calculated values depend strongly on the essentially unknown size of the

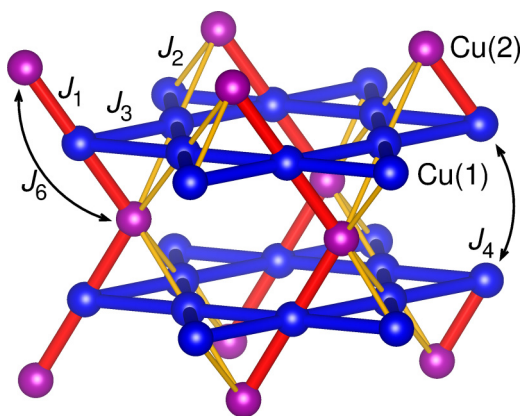


FIG. 4. (Color online) Important exchange paths of  $\text{Cu}_4(\text{OH})_6\text{FBr}$  (see Table II). The notation  $J_i$ ,  $i = 1-6$ , denotes nearest through sixth nearest Cu-Cu neighbors.

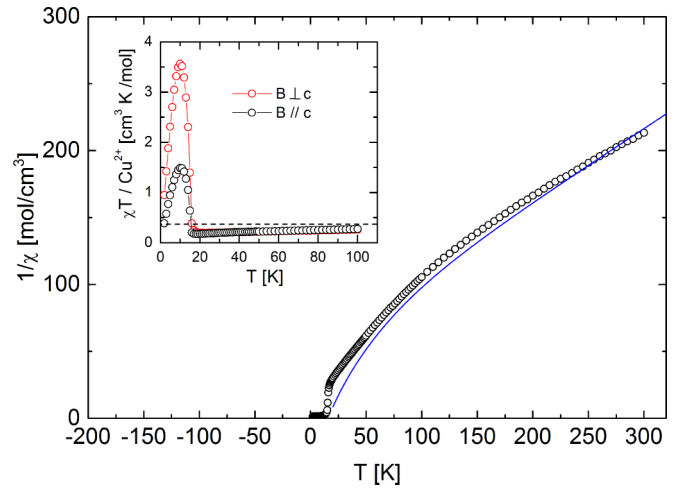


FIG. 5. (Color online) Inverse molar susceptibility as a function of temperature (open circles) taken at  $B = 0.1$  T for  $B \parallel c$  together with a theoretical approximation to  $1/\chi$  calculated by tenth-order high-temperature series expansion [24] (see the main text). Inset:  $\chi_{\text{mol}}T/\text{Cu}^{2+}$  ion as a function of temperature in fields  $B = 0.1$  T for  $B \parallel c$  and  $B \perp c$  both after cooling in zero field (ZFC). The broken line indicates the value for a spin  $S = 1/2$  of 0.376.

Hubbard parameter  $U$  and because of the tendency of DFT to overestimate the stability of the ferromagnetic state.

The magnetic properties of barlowite were measured using a commercial Quantum Design superconducting quantum interference device (SQUID) magnetometer in the temperature range of  $2 \text{ K} \leq T \leq 300 \text{ K}$  on a single crystal of mass  $m = 3.4$  mg. The susceptibility measurements were performed in various fields up to 1 T with orientation parallel and perpendicular to the hexagonal  $c$  axis. For the latter orientation the magnetization was measured in fields up to  $\pm 5$  T. The experimental data have been corrected for the temperature-independent diamagnetic core contribution of the constituents [23] and the magnetic contribution of the sample holder.

By considering the exchange parameters obtained from DFT, we calculated  $1/\chi_{\text{mol}}$  using tenth-order high-temperature series expansion [24]. The result is shown in Fig. 5 together with the experimental  $1/\chi_{\text{mol}}$  data for  $B \parallel c$ . We find that a very good fit of the experimental observations, shown by the solid line, is obtained with  $J_3 = 177$  K and  $J_1 = -0.94J_3$ ,  $J_2 = -0.16J_3$ , and  $J_6 = 0.15J_3$  in combination with a  $g$  value of 2.20. Given the strongly distorted octahedral  $\text{Cu}^{2+}$  environment, implying anisotropic  $g$  values ranging from  $0.1 \leq \Delta g/g \leq 0.15$  [25,26], a  $g$  value of 2.2 for  $B \parallel c$  is reasonable. The so-derived values of the exchange couplings are within the error bars of the DFT calculation confirming that the DFT analysis of barlowite is reliable.

The inset of Fig. 5 exhibits the  $\chi_{\text{mol}}T/\text{Cu}^{2+}$  ion as a function of temperature for  $T \leq 100$  K in fields  $B = 0.1$  T for  $B \parallel c$  and  $B \perp c$  both after ZFC. At 300 K (not shown)  $\chi_{\text{mol}}T$  is about 0.367, a value slightly smaller than the one for isolated spin-1/2 ions. With decreasing temperature  $\chi_{\text{mol}}T$  becomes continuously reduced down to approximately 0.261 around 20 K. Such a large  $\chi_{\text{mol}}T$  value in an antiferromagnetically coupled system at a temperature of  $T \lesssim J_3/10$  is only possible when in addition a ferromagnetic coupling exists which is

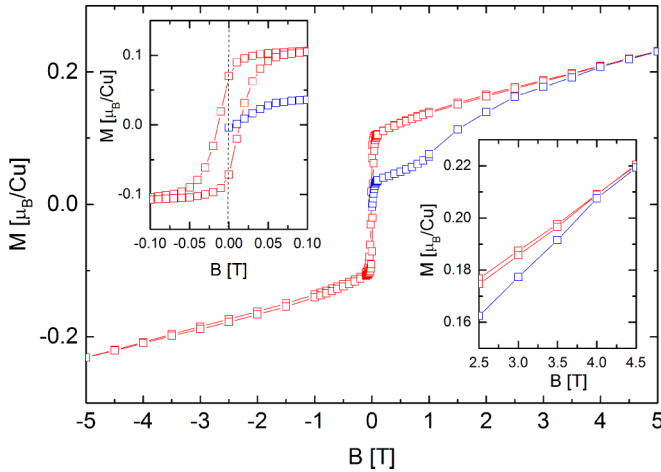


FIG. 6. (Color online) Magnetization as a function of magnetic field  $B$  measured for  $B \parallel c$  at  $T = 2$  K. The blue open squares correspond to the virgin curve taken after cooling in zero field, and the red diamonds correspond to data taken upon subsequent field cycling. Lower right inset: blowup of the high-field section. Upper left inset: blowup of the low-field section.

of similar size. Upon cooling to below about 18 K,  $\chi_{\text{mol}}T$  for both orientations starts to increase with a maximum slope around 15 K, followed by a pronounced maximum. The overall magnetic response, especially the steep increase in  $\chi_{\text{mol}}T$  in the paramagnetic phase close to  $T_N$ , is a clear signature of a phase transition into long-range antiferromagnetic order characterized by canted spins exhibiting a small ferromagnetic component [27]. The maximum of  $\chi_{\text{mol}}T$  for  $B \perp c$  exceeds that for  $B \parallel c$  by more than a factor of 2. These temperature and orientation dependences indicate that the easy axes are tilted against the kagome plane.

Figure 6 exhibits the magnetization measured for  $B \parallel c$  at 2 K. The blue open squares correspond to the virgin curve taken after cooling in zero field. This was possible after carefully compensating for finite remanent fields present in the superconducting magnet of the SQUID magnetometer. Also shown is the full hysteresis loop obtained upon cycling the field in the range of  $-5 \text{ T} \leq B \leq +5 \text{ T}$ . The hysteresis loop closes at  $|B| \geq 4 \text{ T}$  at 2 K, cf. lower right inset in Fig. 6. Upon field cycling (red symbols), following the virgin run, the magnetization exhibits a large slope for fields below 0.1 T. At this field level,  $M$  reaches approximately 10% of the expected saturation magnetization of  $1\mu_B$  per  $\text{Cu}^{2+}$  ion. On further increasing the field  $M(B)$  increases almost linearly and reaches a value of  $0.23\mu_B/\text{Cu}^{2+}$  at 5 T, which is close to  $1\mu_B/\text{f.u.}$  (where f.u. represents formula units). The upper inset of Fig. 6 shows the low-field sector of the hysteresis loop. For  $B = 0$  barlowite has a remanent magnetization of approximately  $0.075\mu_B/\text{Cu}$ . According to

Ref. [23] this value together with the saturation magnetization can be used to determine the tilt angle relative to the perfectly antiferromagnetically aligned spins resulting in a canting angle of approximately  $4.5^\circ$ . We assign the difference between this canting angle and the orientation of the basal plane of the Cu octahedra to the existence of a Dzyaloshinskii-Moriya (DM) interaction allowed by symmetry in barlowite, which acts here like an easy-plane anisotropy. The DM vector  $\mathbf{D}$  lies within the mirror plane [27], which in barlowite is perpendicular to the kagome plane. An estimate of the size of  $|\mathbf{D}|$  is given by  $|\mathbf{D}|/J_3 \simeq \Delta g/g = 0.1$ , which is substantial. As worked out in detail in Ref. [28] the DM interaction in frustrated kagome systems can induce a long-range canted antiferromagnetic order. According to Ref. [28] we can conclude from our experimental findings that  $\mathbf{D}$  is definitely not perpendicular to the kagome plane. In contrast, it has a significant in-plane component  $D_p$ .

According to our calculations, cf. Table II, there are no ferromagnetic interactions between the interlayer Cu(2) ions larger than  $0.1J_1$ , which rules out that the weak ferromagnetism originates from ordering among these interlayer spins. However, the interlayer spins influence the magnetization in the ordered state. There are strong ( $J_1$ ) and moderate ( $J_2$ ) ferromagnetic couplings between the spins on the kagome plane [Cu(1)] and the interlayer spins [Cu(2)]. As a result there are no degrees of freedom left for the Cu(2) spins in fields which are small compared to these couplings. The spins align parallel to the Cu(1) spins belonging to the kagome layers and are thus tilted against the kagome planes. They contribute to the remanent magnetization according to their relative abundance (25%).

To summarize, as exemplarily shown for barlowite, we propose a synthetic route for kagome-based structures with the possibility of interesting phases, such as ordered magnetic phases with different ordering vectors, spin liquid, Dirac metal, or even unconventional superconductivity. On one hand, substitutions at the interlayer cation site [15] may be effective for the realization of such states; on the other hand, the existence of the mineral claringbullite  $\text{Cu}_4(\text{OH})_6\text{FCl}$  [29,30], which is isostructural to barlowite but has different combinations of anions—the  $\text{Br}^-$  ion of barlowite is replaced by  $\text{Cl}^-$ —demonstrates that the synthesis route outlined here opens the path to a family of compounds. Finally, our combined first-principles calculations with susceptibility measurements identify the low-temperature behavior of barlowite as a canted antiferromagnet with a canting angle of approximately  $4.5^\circ$ .

We would like to thank the Deutsche Forschungsgemeinschaft for financial support through the collaborative research center SFB/TRR 49. F.S.-P. gratefully acknowledges the support of the Alexander von Humboldt Foundation through a Humboldt Research Fellowship. J.A.S. acknowledges support from the Independent Research/Development program while serving at the National Science Foundation.

[1] M. P. Shores, E. A. Nytko, B. M. Bartlett, and D. G. Nocera, A. structurally perfect  $S = \frac{1}{2}$  kagomé antiferromagnet, *J. Am. Chem. Soc.* **127**, 13462 (2005).

[2] P. Mendels and F. Bert, Quantum kagome antiferromagnet  $\text{ZnCu}_3(\text{OH})_6\text{Cl}_2$ , *J. Phys. Soc. Jpn.* **79**, 011001 (2010).

- [3] P. Mendels and F. Bert, Quantum kagome antiferromagnet:  $\text{ZnCu}_3(\text{OH})_6\text{Cl}_2$ , *J. Phys.: Conf. Ser.* **320**, 012004 (2011).
- [4] S.-H. Lee, H. Kikuchi, Y. Qiu, B. Lake, Q. Huang, K. Habicht, and K. Kiefer, Quantum-spin-liquid states in the two-dimensional kagome antiferromagnets  $\text{Zn}_x\text{Cu}_{4-x}(\text{OD})_6\text{Cl}_2$ , *Nat. Mater.* **6**, 853 (2007).
- [5] R. H. Colman, A. Sinclair, and A. S. Wills, Magnetic and crystallographic studies of Mg-herbertsmithite,  $\gamma\text{-Cu}_3\text{Mg}(\text{OH})_6\text{Cl}_2$ —A new  $S = 1/2$  kagome magnet and candidate spin liquid, *Chem. Mater.* **23**, 1811 (2011).
- [6] Y. Li, B. Pan, S. Li, W. Tong, L. Ling, Z. Yang, J. Wang, Z. Cheng, Z. Wu, and Q. Zhang, Gapless quantum spin liquid in the  $S = 1/2$  anisotropic kagome antiferromagnet  $\text{ZnCu}_3(\text{OH})_6\text{SO}_4$ , *New J. Phys.* **16**, 093011 (2014).
- [7] Y.-S. Li and Q.-M. Zhang, Structure and magnetism of  $S = 1/2$  kagome antiferromagnets  $\text{NiCu}_3(\text{OH})_6\text{Cl}_2$  and  $\text{CoCu}_3(\text{OH})_6\text{Cl}_2$ , *J. Phys.: Condens. Matter* **25**, 026003 (2013).
- [8] P. A. Lee, An end to the drought of quantum spin liquids, *Science* **321**, 1306 (2008).
- [9] Y. Shimizu, K. Miyagawa, K. Kanoda, M. Maesato, and G. Saito, Spin Liquid State in an Organic Mott Insulator with a Triangular Lattice, *Phys. Rev. Lett.* **91**, 107001 (2003).
- [10] T. Itou, A. Oyamada, S. Maegawa, M. Tamura, and R. Kato, Quantum spin liquid in the spin-1/2 triangular antiferromagnet  $\text{EtMe}_3\text{Sb}[\text{Pd}(\text{dmit})_2]_2$ , *Phys. Rev. B* **77**, 104413 (2008).
- [11] T.-H. Han, J. S. Helton, S. Chu, D. G. Nocera, J. A. Rodriguez-Rivera, C. Broholm, and Y. S. Lee, Fractionalized excitations in the spin-liquid state of a kagome-lattice antiferromagnet, *Nature (London)* **492**, 406 (2012).
- [12] D. E. Freedman, T. H. Han, A. Prodi, Peter Müller, Q.-Z. Huang, Y.-S. Chen, S. M. Webb, Y. S. Lee, T. M. McQueen, and D. G. Nocera, Site specific x-ray anomalous dispersion of the geometrically frustrated kagomé magnet, herbertsmithite,  $\text{ZnCu}_3(\text{OH})_6\text{Cl}_2$ , *J. Am. Chem. Soc.* **132**, 16185 (2010).
- [13] T.-H. Han, J. Singleton, and J. A. Schlueter, Barlowite: A Spin-1/2 Antiferromagnet with a Geometrically Perfect Kagome Motif, *Phys. Rev. Lett.* **113**, 227203 (2014).
- [14] T. Hanisch, G. S. Uhrig, and E. Müller-Hartmann, Lattice dependence of saturated ferromagnetism in the Hubbard model, *Phys. Rev. B* **56**, 13960 (1997).
- [15] I. I. Mazin, H. O. Jeschke, F. Lechermann, H. Lee, M. Fink, R. Thomale, and R. Valentí, Theoretical prediction of a strongly correlated Dirac metal, *Nat. Commun.* **5**, 4261 (2014).
- [16] P. Elliott and M. A. Cooper, New minerals and nomenclature modifications approved in 2010, *Mineral. Mag.* **74**, 797 (2010).
- [17] CCDC 1019246 contains the supplementary crystallographic data for this paper. These data can be obtained free of charge from The Cambridge Crystallographic Data Centre via [www.ccdc.cam.ac.uk/data\\_request/cif](http://www.ccdc.cam.ac.uk/data_request/cif)
- [18] K. Koepernik and H. Eschrig, Full-potential nonorthogonal local-orbital minimum-basis band-structure scheme, *Phys. Rev. B* **59**, 1743 (1999), <http://www.FPLO.de>.
- [19] J. P. Perdew, K. Burke, and M. Ernzerhof, Generalized Gradient Approximation Made Simple, *Phys. Rev. Lett.* **77**, 3865 (1996).
- [20] A. I. Liechtenstein, V. I. Anisimov, and J. Zaanen, Density functional theory and strong interactions: Orbital ordering in Mott-Hubbard insulators, *Phys. Rev. B* **52**, R5467 (1995).
- [21] H. O. Jeschke, F. Salvat-Pujol, and R. Valentí, First-principles determination of Heisenberg Hamiltonian parameters for the spin-1/2 kagome antiferromagnet  $\text{ZnCu}_3(\text{OH})_6\text{Cl}_2$ , *Phys. Rev. B* **88**, 075106 (2013).
- [22] K. Foyevtsova, I. Oshale, Y.-Z. Zhang, H. O. Jeschke, and R. Valentí, Determination of effective microscopic models for the frustrated antiferromagnets  $\text{Cs}_2\text{CuCl}_4$  and  $\text{Cs}_2\text{CuBr}_4$  by density functional methods, *Phys. Rev. B* **83**, 125126 (2011).
- [23] O. Kahn, *Molecular Magnetism* (VCH, Weinheim-New York, 1993).
- [24] A. Lohmann, H.-J. Schmidt, and J. Richter, Tenth-order high-temperature expansion for the susceptibility and the specific heat of spin- $s$  Heisenberg models with arbitrary exchange patterns: Application to pyrochlore and kagome magnets, *Phys. Rev. B* **89**, 104415 (2014).
- [25] B. L. Silver and D. Getz, ESR of  $\text{Cu}^{2+}(\text{H}_2\text{O})_6$ . II. A quantitative study of the dynamic Jahn-Teller effect in copper-doped zinc Tutton's salt, *J. Chem. Phys.* **61**, 638 (1973).
- [26] V. E. Petrashen, Yu. V. Yablokov, and R. L. Davidovich, The lattice structure parameters and configuration of  $\text{Cu}^{2+}$  Jahn-Teller centres in Tutton salt crystals, *Phys. Status Solidi B* **101**, 117 (1980).
- [27] T. Moriya, Anisotropic superexchange interaction and weak ferromagnetism, *Phys. Rev.* **120**, 91 (1960).
- [28] M. Elhajal, B. Canals, and C. Lacroix, Symmetry breaking due to Dzyaloshinsky-Moriya interactions in the kagomé lattice, *Phys. Rev. B* **66**, 014422 (2002).
- [29] E. E. Fejer, A. M. Clark, A. G. Couper, and C. J. Elliott, Claringbullite, a new hydrated copper chloride, *Mineral. Mag.* **41**, 433 (1977).
- [30] M. S. Rumsey, M. D. Welch, M. J. Origlieri, G. Cressey, A. R. Kampf, L. Burgio, J. Spratt, and E. R. Humphreys-Williams, in *A redefinition of claringbullite to  $\text{Cu}_4\text{ClF}(\text{OH})_6$ : the importance of type material and group/series based studies*, 21st General Meeting of the International Mineralogical Association, Sandton, Johannesburg, South Africa, 2014 (IMA, 2014), Abstract volume, p. 375.